

## **Electronic Supplementary Information**

### **Annealing-free aqueous-processed anatase TiO<sub>2</sub> compact layer for efficient planar heterojunction perovskite solar cells**

Chengwu Yang,<sup>a</sup> Mingyu Yu,<sup>a</sup> Dichun Chen,<sup>b</sup> Yaqing Zhou,<sup>a</sup> Wei Wang,<sup>a</sup> Yang Li,<sup>a</sup>  
Tung-Chun Lee<sup>\*c</sup> and Daqin Yun<sup>\*a</sup>

<sup>a</sup>. College of Energy, Xiamen University, Xiamen 361002, China. E-mail: [dqyun@xmu.edu.cn](mailto:dqyun@xmu.edu.cn)

<sup>b</sup>. Xiamen Branch of Luoyang Ship Material Research Institute, Xiamen, 361006, China.

<sup>c</sup>. Department of Chemistry and Institute for Materials Discovery, University College London (UCL), United Kingdom.  
E-mail: [tungchun.lee@ucl.ac.uk](mailto:tungchun.lee@ucl.ac.uk)

### **Experimental Section**

#### **Materials**

Lead (II) iodide (99.999%) was purchased from Alfa-Aesar. Titanium (IV) isopropoxide (TTIP) (97%), Titanium diisopropoxide bis(acetylacetonate)(TiACAC) (75wt.% in isopropanol), formamidinium acetate salt (99%), methylamine (CH<sub>3</sub>NH<sub>2</sub>) solution (33 wt.% in absolute ethanol), hydroiodic acid (HI) (57 wt.% in H<sub>2</sub>O), anhydrous dimethylformamide (DMF) (99.8%), methylamine hydrochloride (MACI), anhydrous dimethylsulfoxide (DMSO) (99.9%), acetonitrile(99.8%), 4-tertbutyl pyridine (4-tBP, 96%), and bis(trifluoromethane) sulfonimide lithium salt (Li-TFSI) (99.95%) were purchased from Sigma-Aldrich. 2,2',7,7'-tetrakis-(N,N-di-p-methoxyphenylamine)9,9'-spirobifluorene (Spiro-OMeTAD) was received from Ossila. Tris(2-(1H-pyrazol-1-yl)-4-tert-butylpyridine)-cobalt(III) tris-(bis(trifluoromethylsulfonyl)imide)) (FK209) was purchased from Dyenanmo AB. Other reagents and chemicals were used as received without further purification unless otherwise noted.

#### **Synthesis of annealing-free nanocrystalline anatase TiO<sub>2</sub> (AF-TiO<sub>2</sub>) nanoparticles**

AF-TiO<sub>2</sub> nanoparticles was prepared by a hydrolytic sol-gel method based on a modified procedure from a previous report.<sup>1</sup> Briefly, TTIP (35 mM) mixed with isopropyl alcohol was slowly added dropwise to 120 mL deionized water mixed with nitric acid under continuous vigorous stirring for 30 min at room temperature. Subsequently, white colloidal solution of TiO<sub>2</sub> NPs were

formed after hydrolysis and the solution was heated to 80°C and stirred vigorously for 4 h to yield a nanocrystalline TiO<sub>2</sub> NP solution with a concentration of 20 mg mL<sup>-1</sup>. Before use, the TiO<sub>2</sub> NPs solution was filtered through a 0.45 µm PVDF syringe filter.

#### **Synthesis of the organo-metal halide perovskite**

Formamidinium iodide (NH<sub>2</sub>CH=NH<sub>2</sub>I,FAI) was synthesized by reacting 0.3 mol formamidine acetate dissolved in 40 mL anhydrous ethanol and 40 mL equimolar HI in a 250 mL round-bottomed flask at room temperature for 2 h with stirring.<sup>2</sup> Similarly, methylammonium iodide (CH<sub>3</sub>NH<sub>3</sub>I,MAI) was prepared by 0.3 mol (38 mL) methylamine (CH<sub>3</sub>NH<sub>2</sub>) solution (33 wt% in absolute ethanol) was reacted with equimolar (40 mL) hydroiodic acid (HI) (57% in water) in a 250 mL round-bottomed flask at 0 °C for 2 h with stirring.<sup>3</sup> The precipitate was collected by putting the solution on a rotary evaporator and carefully removing the solvents at 50 °C, which were then dissolved in ethanol and recrystallized using diethyl ether. The process was repeated three times, and the product was finally dried at 60 °C in a vacuum oven for 24 h. The product was then kept in an inert atmosphere glovebox until further use.

#### **Synthesis of PbI<sub>2</sub>(DMSO)**

The preparation of the PbI<sub>2</sub>(DMSO) complex was similar to that reported.<sup>4</sup> PbI<sub>2</sub> (20 g) was dissolved in DMSO of 60 mL at 60 °C and then toluene of 140 mL was slowly added into the PbI<sub>2</sub> solution. The white PbI<sub>2</sub>(DMSO)<sub>2</sub> precipitate was filtered, dried for 2 h at room temperature and then annealed at 60 °C in vacuum oven for 24 h to obtain the PbI<sub>2</sub>(DMSO) complex.

#### **Fabrication of solar cells with AF-TiO<sub>2</sub> and two types of control samples (LT-TiO<sub>2</sub> and HTA-TiO<sub>2</sub>)**

Planar heterojunction PSCs with a configuration of ITO/TiO<sub>2</sub> compact layer/Perovskite/Spiro-OMeTAD/Ag were fabricated. A patterned ITO glass substrate was cleaned by sequential ultrasonic treatment in detergent, deionized water, acetone, and isopropyl alcohol. The anatase TiO<sub>2</sub> NPs were spin coated onto the ITO substrate at 4000 rpm for 50 s, to yield an annealing-free anatase TiO<sub>2</sub> (AF-TiO<sub>2</sub>) compact layer. To investigate the effect of low-temperature annealing, a series of control samples were annealed in air under ambient pressure at 120 °C for 60 min (LT-TiO<sub>2</sub>). The thickness of the TiO<sub>2</sub> compact layer was tuned by adjusting the number of the above spin-coating cycle. For comparison, a compact layer of amorphous TiO<sub>2</sub> treated by

high-temperature annealing (**HTA-TiO<sub>2</sub>**) was prepared by spin-coating a TiACAC precursor solution in anhydrous ethanol (0.15 M) on the FTO substrate, followed by sintering at 500 °C for 30 min according to a standard control procedure.<sup>5</sup> The following coating steps were performed under argon atmosphere inside a glovebox. For the perovskite layer, 1.50 M PbI<sub>2</sub>(DMSO) complex solution in DMF was preheated at 70 °C. The PbI<sub>2</sub>(DMSO) complex solution was spin coated on top of the TiO<sub>2</sub> layer at 2000 rpm for 45 s. Subsequently, 60 mgmL<sup>-1</sup> MAI, FAI, or a mixture of FAI:MAI (molar ratio of FAI / MAI was 3.92) solution in 2-propanol was spin coated top of the PbI<sub>2</sub>(DMSO) film at 2000 rpm for 40 s. The substrates were then annealed on a hot plate at 120 °C for desired period of time. After cooling to room temperature, Spiro-OMeTAD was then deposited on top of the perovskite layer by spin-coated at 2000 rpm for 40 s. The Spiro-OMeTAD solution was prepared by dissolving Spiro-OMeTAD in chlorobenzene (60 mM), with the addition of 30 mM Li-TFSI (520 mg mL<sup>-1</sup> in acetonitrile), 200 mM 4-tBP, and 1.8 mM FK209 (300 mg mL<sup>-1</sup> in acetonitrile). Finally, 150 nm of silver was deposited by thermal evaporation using a shadow mask to pattern the electrodes at a base pressure of 4 ×10<sup>-4</sup> Pa; the active area of this electrode was fixed at 0.12 cm<sup>2</sup>.

### **Characterisation**

The current-density-voltage (*J*-*V*) characteristics of photovoltaic cells were performed using a 300 W xenon solar simulator (Newport Oriel Solar Simulators) with a source meter (Keithley 2420, USA) under the illumination of AM 1.5 G, 100 mW cm<sup>-2</sup>, and a calibrated Si-reference cell. Unless stated otherwise, the *J*-*V* curves were measured by forward scan (short circuit (-0.1 V) to forward bias (1.2 V)). The step voltage was fixed at 100 mV. The incident photon-to-electron conversion efficiency (IPCE) / external quantum efficiency (EQE) was measured with a power source (66920, Newport, 300 W xenon lamp) with a monochromator (Cornerstone 260, Newport) and an optical power meter (2936-R, Newport). All the devices were characterised in air (humidity ranging from 40% to 50% and temperature 22 °C). High-resolution TEM images were taken on a JEOL JEM2100 transmission electron microscope operated at 300 kV. The diluted TiO<sub>2</sub> nanocrystals solution was dropped onto the copper mesh and dried, after which the sample was loaded into the TEM chamber for measurement. The morphologies were investigated by field-emission scanning electron microscopy (SEM) (SUPRA 55). The XRD spectra of TiO<sub>2</sub>

nanocrystals and perovskite films were measured using Rigaku Ultima IV X-ray diffractometer. The absorption spectra of the samples were recorded using a spectrophotometer (UV-2550, Shimadzu). Steady Photoluminescence (PL) was obtained using an F7000 Fluorescence Spectrometer (HITACHI). Electrochemical impedance spectroscopy (EIS) measurements were performed on Princeton multifunctional electrochemical workstation (VersaSTAT) in the dark at a DC bias of 0 – 0.8 V. A 20-mV AC signal was applied with a frequency range of 0.01 Hz to 100 kHz. The thickness of the thin films was determined by a KLA-Tencor Alpha-Step Surface Profiler.

### Statistical analysis

To investigate the effects of anatase TiO<sub>2</sub> layer thickness on device performance, a series of devices were prepared by spin coating one, two, three, four and five layers of anatase TiO<sub>2</sub> NPs (Fig. S1 and Table S1). For each PSC design (AF-TiO<sub>2</sub> films with a different layer thickness, the corresponding LT-TiO<sub>2</sub> films and the HTA-TiO<sub>2</sub> films), 10 independent devices were fabricated to obtain statistical significant measurement data<sup>6</sup> as summarised in Fig. S8, Table 1 and S1. The data verifies the high reproducibility of our fabrication scheme.

### References

- [1] C. J. Barbé, F. Arendes, P. Comte, M. Jirousek, F. Lenzmann, V. Shklover, M. Grätzel, *J. Am. Ceram. Soc.*, **80**, 3157-3171.
- [2] G. E. Eperon, S. D. Stranks, C. Mebelaou, M. B. Johnston, L. M. Herz, H. J. Snaith, *Energy Environ. Sci.*, 2014, **7**, 982-988.
- [3] H. Zhou, Q. Chen, G. Li, S. Luo, T. Song, H. Duan, Z. Hong, J. You, Y. Liu, Y. Yang, *Science*, 2014, **345**, 542-546.
- [4] W. S. Yang, J. H. Noh, N. J. Jeon, Y. C. Kim, S. Ryu, J. Seo, S. I. Seok, *Science*, 2015, **348**, 1234-1237.
- [5] Y. Zhao, J. Wei, H. Li, Y. Yan, W. Zhou, D. Yu, Q. Zhao, *Nat. Commun.*, 2016, **7**, 10228.
- [6] Q. Chen, H. Zhou, Y. Fang, A. Z. Stieg, T. Song, H. Wang, X. Xu, Y. Liu, S. Lu, J. You, P. Sun, J. Mckay, M. S. Goorsky, Y. Yang, *Nat. Commun.*, 2015, **6**, 7269.

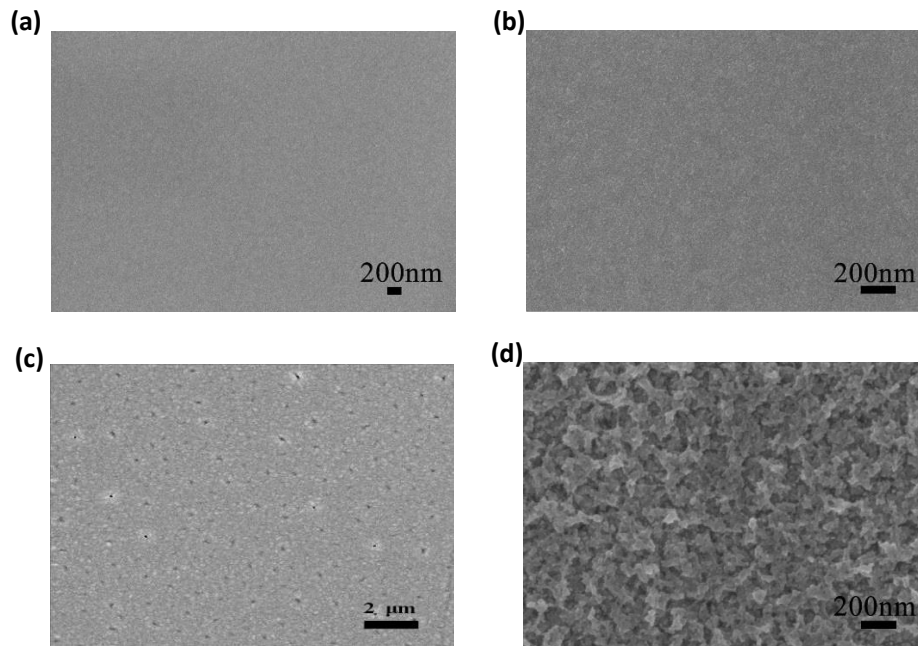


**Fig. S1.** (a), (b) Top-view SEM image of AF-TiO<sub>2</sub> film deposited on a glass/ITO substrate under different magnification. (c), (d) Top-view SEM image of HTA-TiO<sub>2</sub> film deposited on a glass/FTO substrate with annealing at 500 °C for 30 min under different magnification.

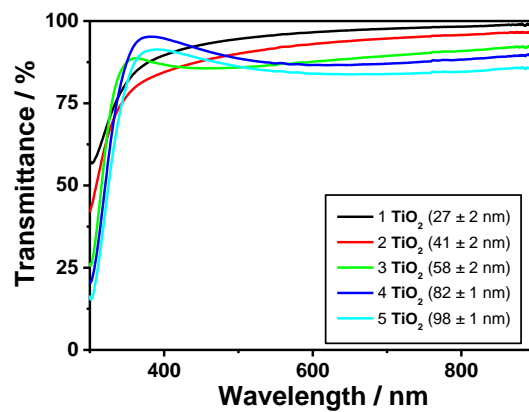


**Fig. S2.** Transmittance measurements of AF-TiO<sub>2</sub> films with a different thickness. The number before “TiO<sub>2</sub>” in the legend indicates the number of TiO<sub>2</sub> NP layers spin coated on the substrate.

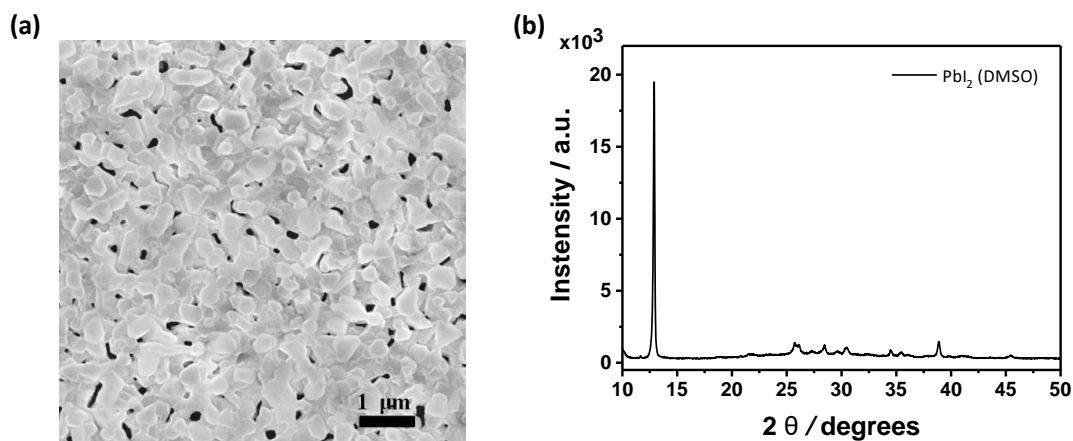


**Fig. S3.** (a) SEM image of  $\text{PbI}_2(\text{DMSO})$  film. (b) XRD of  $\text{PbI}_2(\text{DMSO})$  film.

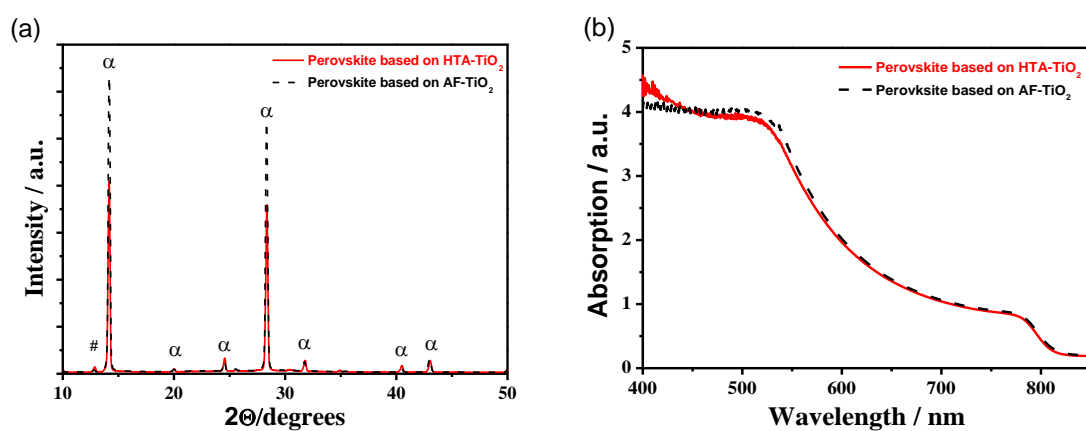


**Fig. S4.** (a) XRD of  $(\text{FAPbI}_3)_x(\text{MAPbCl}_3)_{1-x}$  films on  $\text{AF-TiO}_2$  and  $\text{HTA-TiO}_2$  substrates. # and  $\alpha$  denote the identified diffraction peaks corresponding to  $\text{PbI}_2$  and  $(\text{FAPbI}_3)_x(\text{MAPbCl}_3)_{1-x}$ , respectively. The stronger diffraction peaks of perovskite based on  $\text{AF-TiO}_2$  verify the formation of larger crystal grains, compared to the case of  $\text{HTA-TiO}_2$ . (b) Absorption spectra of  $(\text{FAPbI}_3)_x(\text{MAPbCl}_3)_{1-x}$  films on  $\text{AF-TiO}_2$  and  $\text{HTA-TiO}_2$  substrates. The similar absorption spectra indicate both perovskite active layers have almost the same thickness.

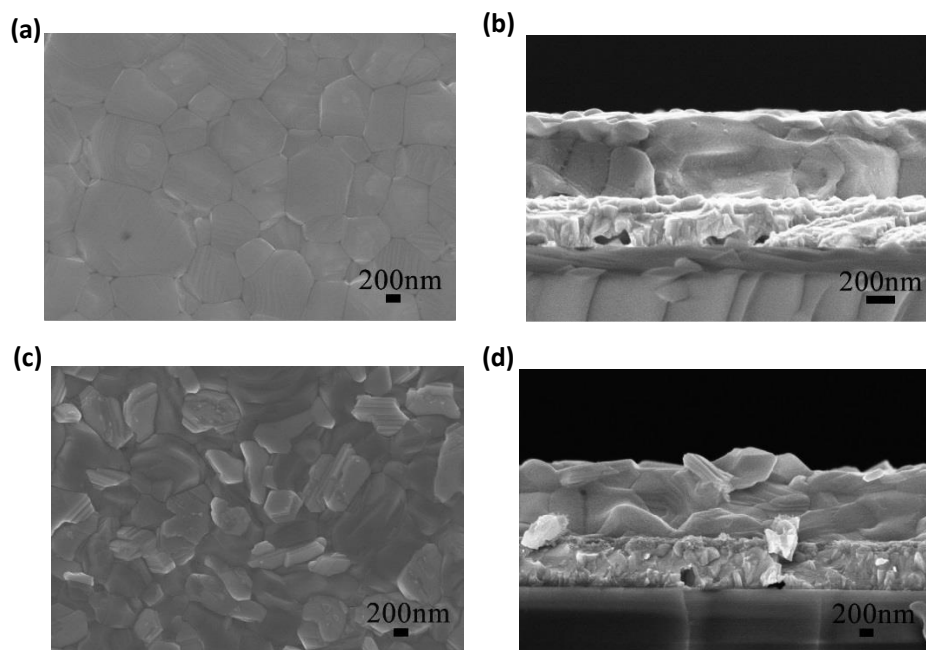


**Fig. S5.** (a) Top-view and (b) cross-section SEM images of  $(\text{FAPbI}_3)_x(\text{MAPbCl}_3)_{1-x}$  film on AF-TiO<sub>2</sub>, showing a smooth and compact morphology. (c) Top-view and (d) cross-section SEM images of  $(\text{FAPbI}_3)_x(\text{MAPbCl}_3)_{1-x}$  film on HTA-TiO<sub>2</sub>, showing a coarse-grain morphology.

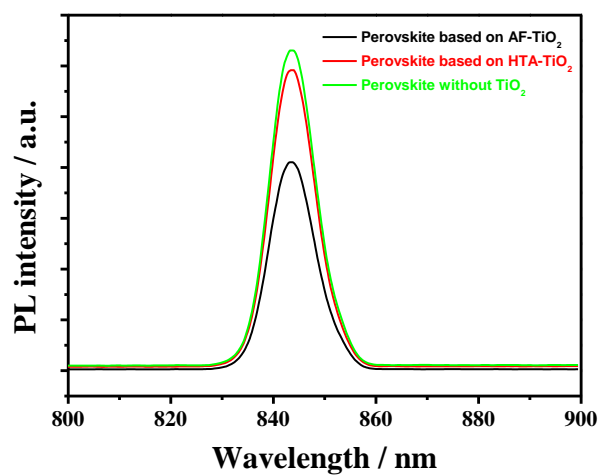


**Fig. S6.** Photoluminescence (PL) spectra of perovskite based on AF-TiO<sub>2</sub>, HTA-TiO<sub>2</sub> and without TiO<sub>2</sub> ETL. A significant PL quenching indicates efficient electron transfer from perovskite to AF-TiO<sub>2</sub>.

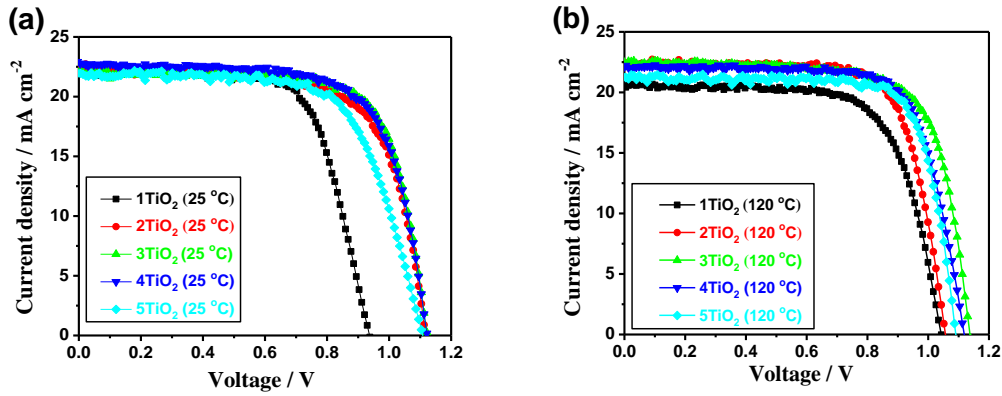


**Fig. S7.** (a)  $J$ - $V$  curves of typical PSCs with different thicknesses of AF-TiO<sub>2</sub> films and (b) of LT-TiO<sub>2</sub> films. The number before “TiO<sub>2</sub>” in the legend indicates the number of TiO<sub>2</sub> NP layers spin coated on the substrate.

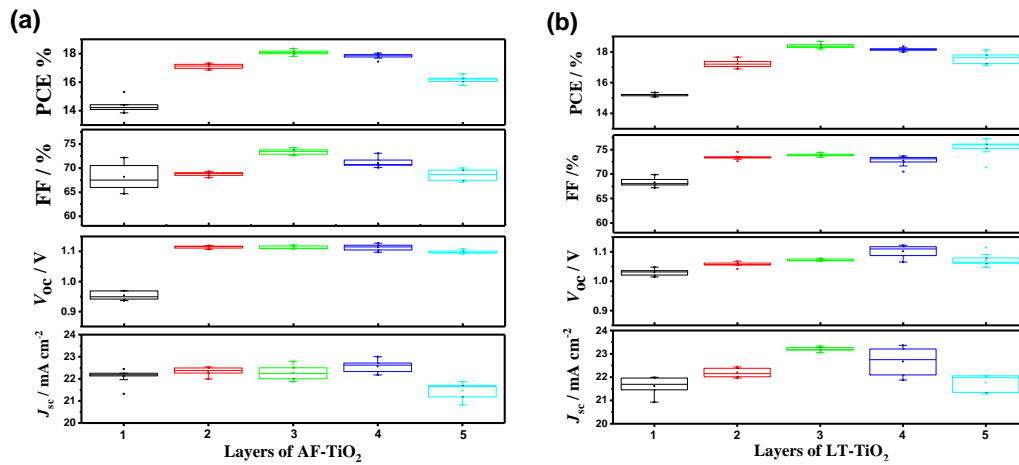


**Fig. S8.** Statistical distribution of photovoltaic parameters including  $V_{oc}$ ,  $J_{sc}$ , FF, and PCE, extracted from  $J$ - $V$  measurements of the perovskite solar cells based on (a) AF-TiO<sub>2</sub> films and (b) LT-TiO<sub>2</sub> films under simulated AM 1.5 ( $100 \text{ mW cm}^{-2}$ ) illumination. Horizontal lines in the box indicate the average photovoltaic parameters of PSCs.<sup>6</sup>

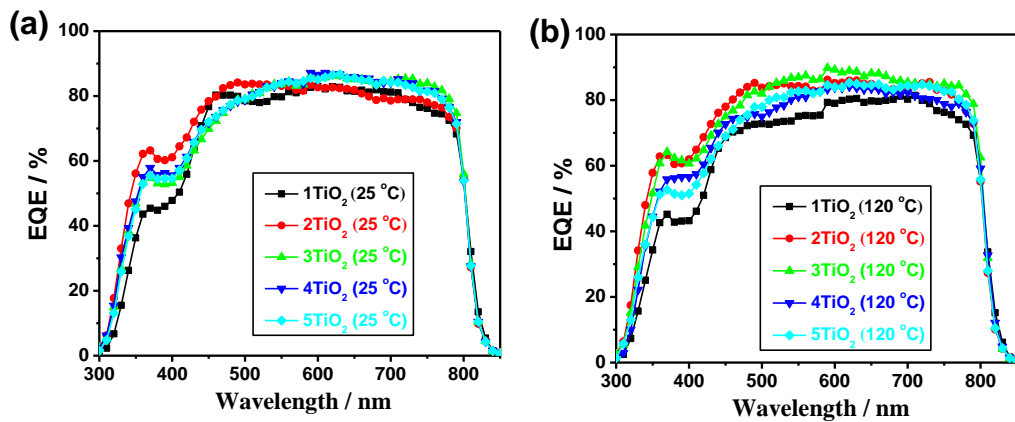


**Fig. S9.** EQE spectra of typical PSCs with a different thickness of (a) AF-TiO<sub>2</sub> films and of (b) LT-TiO<sub>2</sub> films. The number before “TiO<sub>2</sub>” in the legend indicates the number of TiO<sub>2</sub> NP layers spin coated on the substrate.



**Table S1.** Photovoltaic parameters of PSCs based on AF-TiO<sub>2</sub> (25 °C) films and LT-TiO<sub>2</sub> (120 °C) films measured under simulated AM 1.5 (100 mW cm<sup>-2</sup>) illumination. Series resistance is derived from *J-V* curve (Fig. S7). Statistical analysis is based on measurement of 10 individual devices. “Champion” refers to the measurement data of the device with the highest PCE. Optimal PCE (18.29 ± 0.18 %) can be achieved by 3 spin-coating cycles (ETL thickness = 58 ± 2 nm). Fewer cycles will result in a discontinuous film as indicated by the increase in series resistance, while more cycles will lead to a thicker film with increasing *R<sub>s</sub>* and decreasing optical transmittance.

No. of layers (Temp.)	TiO <sub>2</sub> thickness* (nm)		<i>J<sub>sc</sub></i> (mA cm <sup>-2</sup> )	<i>V<sub>oc</sub></i> (V)	Fill factor (%)	PCE (%)	Series resistance (Ω cm <sup>2</sup> )
1 (25 °C)	27±2	champion	22.10	0.95	69.54	14.53	7.83
		average	22.00 ± 0.32	0.95 ± 0.01	67.80 ± 2.31	14.20 ± 0.22	9.78 ± 1.76
1 (120 °C)		champion	21.94	1.03	67.97	15.35	6.38
		average	21.61 ± 0.40	1.03 ± 0.01	68.29 ± 0.84	15.20 ± 0.09	7.15 ± 0.45
2 (25 °C)	41±2	champion	22.37	1.11	70.62	17.58	4.88
		average	22.29 ± 0.21	1.11 ± 0.01	69.07 ± 0.86	17.13 ± 0.28	5.48 ± 0.62
2 (120 °C)		champion	22.42	1.05	74.52	17.64	5.54
		average	22.19 ± 0.20	1.05 ± 0.01	73.44 ± 0.50	17.21 ± 0.24	5.70 ± 0.17
3 (25 °C)	58±2	champion	22.41	1.10	74.87	18.50	4.49
		average	22.27 ± 0.19	1.11 ± 0.01	73.63 ± 0.86	18.29 ± 0.18	4.79 ± 0.20
3 (120 °C)		champion	23.29	1.08	74.42	18.67	4.85
		average	23.20 ± 0.08	1.07 ± 0.01	73.88 ± 0.30	18.37 ± 0.14	4.69 ± 0.17
4 (25 °C)	82±1	champion	22.58	1.10	72.54	18.12	4.89
		average	22.43 ± 0.41	1.11 ± 0.01	71.61 ± 1.15	17.83 ± 0.14	4.97 ± 0.26
4 (120 °C)		champion	22.50	1.12	72.68	18.35	6.05
		average	22.67 ± 0.56	1.10 ± 0.02	72.73 ± 0.98	18.15 ± 0.11	5.51 ± 0.67
5 (25 °C)	98±1	champion	21.81	1.13	71.70	17.73	5.89
		average	21.82 ± 0.28	1.11 ± 0.01	70.63 ± 0.92	17.17 ± 0.33	5.17 ± 0.46
5 (120 °C)		champion	21.99	1.07	75.92	17.86	4.46
		average	21.76 ± 0.35	1.07 ± 0.02	75.41 ± 1.60	17.57 ± 0.34	4.67 ± 0.18

\*Thickness of the TiO<sub>2</sub> films was measured by a surface profilometer, consistent with the thickness determined by SEM.

**Table S2.** Photovoltaic parameters extracted from Fig. 3d.

Compact layer (Anneal Temp.)	<i>J<sub>sc</sub></i> (mA cm <sup>-2</sup> )	<i>V<sub>oc</sub></i> (V)	FF (%)	PCE (%)	Series resistance (Ω cm <sup>2</sup> )
FS AF-TiO <sub>2</sub> (25 °C)	22.00	1.12	73.30	18.09	4.94
RS AF-TiO <sub>2</sub> (25 °C)	22.39	1.10	65.96	16.33	6.36

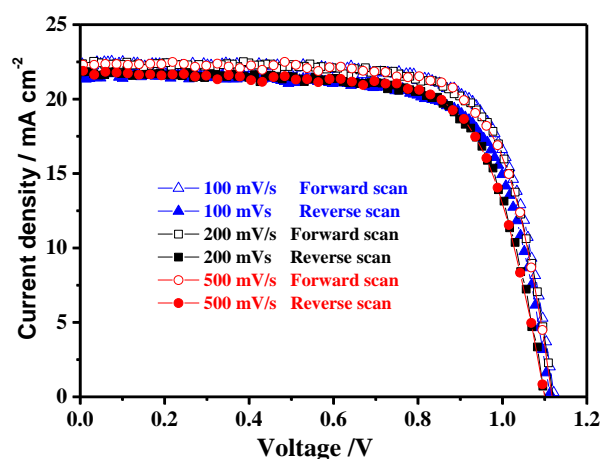


**Fig. S10.** *J*-*V* curves of an optimised AF-TiO<sub>2</sub>-based device under different scan directions and scan rates. The different scan directions show almost the same performance.

**Table S3.** Performance parameters of an AF-TiO<sub>2</sub>-based device based on the optimised thickness of AF-TiO<sub>2</sub> under different scan conditions. Photovoltaic parameters extracted from Fig. S10.

Scan direction	Scan rate	$V_{oc}$ (V)	$J_{sc}$ (mA/cm <sup>2</sup> )	FF (%)	PCE (%)
Forward	100mV/s	1.12	22.37	73.34	18.41
Reverse	100mV/s	1.11	21.57	71.56	17.18
Forward	200mV/s	1.12	22.39	72.56	18.17
Reverse	200mV/s	1.10	21.75	70.99	16.97
Forward	500mV/s	1.11	22.37	73.01	18.22
Reverse	500mV/s	1.10	21.75	71.28	17.07

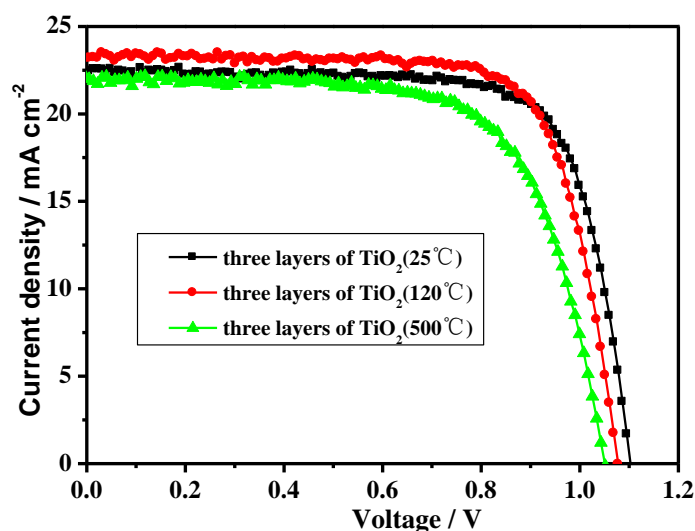


**Fig. S11.** *J*-*V* curves of the champion PSCs based on 25 °C, 120 °C and 500 °C annealed TiO<sub>2</sub> nanocrystalline films. An additional low-temperature annealing step at 120 °C generally enhances the PSC performance. However, the improvement is marginal because this temperature can only

induce desorption of small molecules (e.g. water) from TiO<sub>2</sub> surface but not sufficient to trigger largescale sintering and recrystallisation of anatase TiO<sub>2</sub> which typically occur above 450 °C. The decrease in PV performance after annealing at 500 °C is due to the formation of cracks between the growing crystal grains in the ETL.

**Table S4.** Detailed parameters of PSCs based on 25 °C, 120 °C and 500 °C annealed TiO<sub>2</sub> nanocrystalline films. Photovoltaic parameters extracted from Fig. S11.

No. of Layers (Temp.)	TiO <sub>2</sub> thickness (nm)	$J_{sc}$ (mAcm <sup>-2</sup> )	$V_{oc}$ (V)	Fill factor (%)	PCE (%)
3 (25 °C)	champion	22.41	1.10	74.87	18.50
	average	58± 2	22.27±0.19	1.11±0.01	73.63±0.86
3 (120 °C)	champion	23.29	1.08	74.42	18.67
	average	58± 2	23.20 ±0.08	1.07±0.01	73.88±0.30
3 (500°C)	champion	21.98	1.05	67.99	15.70
	average	58± 2	21.88±0.56	1.01±0.02	65.13±2.8

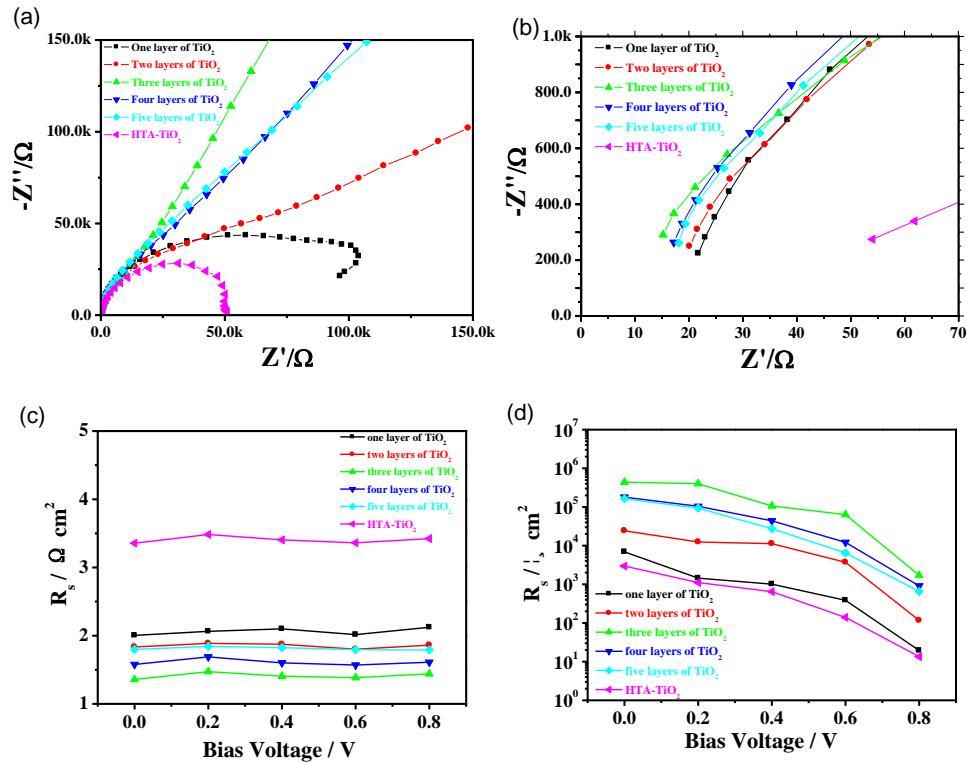


**Fig. S12.** (a) Nyquist plots of PSCs based on different TiO<sub>2</sub> electronic transport layers in the dark at a DC bias of 0 V. A 20-mV AC signal was applied with a frequency range of 0.01 Hz to 100 kHz. (b) Nyquist plots of the high frequency region. (c) Series resistance ( $R_s$ ) as a function of bias. (d) Interfacial charge-recombination resistance ( $R_{rec}$ ) as a function of bias.